Materials Sciences and Applications, 2011, 2, 258-264
doi:10.4236/msa.2011.24033 Published Online April 2011 (http://www.scirp.org/journal/msa)

Scientific Research

NiO_x Nanoparticle Synthesis by Chemical Vapor Deposition from Nickel Acetylacetonate

Pavel Moravec[1], Jiří Smolík[1], Helmi Keskinen[2,3], Jyrki M. Mäkelä[2], Snejana Bakardjieva[4], Valeri V. Levdansky[5]

[1]Institute of Chemical Process Fundamentals AS CR, Prague, Czech Republic; [2]Department of Physics, Tampere University of Technology, Tampere, Finland; [3]Department of Physics and Mathematics, University of Eastern Finland, Kuopio, Finland; [4]Institute of Inorganic Chemistry AS CR, Husinec-Řež, Czech Republic; [5]A. V. Luikov Heat and Mass Transfer Institute, National Academy of Sciences of Belarus, Minsk, Belarus
Email: moravec@icpf.cas.cz, helmi.keskinen@uef.fi

Received November 4th, 2010; revised January 17th, 2011; accepted March 9th, 2011.

ABSTRACT

Ni/NiO nanoparticles were synthesized by metal organics chemical vapor deposition of nickel acetylacetonate in an externally heated tube flow reactor at moderate temperatures, up to 500˚C. Particle production and characteristics were studied by evaluating the effects of reactor temperature, precursor concentration, and flow rate through the reactor. In addition, two precursor decomposition methods were examined: thermal decomposition and reduction by hydrogen. Particle production was monitored with a scanning mobility particle sizer, and particle characteristics were studied using transmission electron microscopy, high resolution transmission electron microscopy, selected area electron diffraction, and energy dispersive spectroscopy. The presence of hydrogen in the reaction mixture influenced significantly both particle production and their characteristics.

***Keywords*:** *Nickel Nanostructures*, *MOCVD*, *Hot Wall Tube Reactor*, *Electron Diffraction*

1. Introduction

Nickel and nickel oxide nanoparticles show many unique optical, magnetic, electrical and chemical properties [1,2], and thus, these nanoparticles have great potential in applications such as ceramic materials, electronic components, sensors, magnetic data storage materials and catalysts [3,4]. However, most physical and chemical properties depend on the size and shape of the nanoparticles [5]. Moreover, nickel nanoparticles are unstable in air, and their surface can oxidize to NiO even at room temperature [6].

In recent years, several methods of Ni/NiO nanoparticle synthesis have been reported and, of course, each different method of synthesis imparts the final product with different properties. Liquid phase synthesis is one subset of methods for synthesizing Ni/NiO [7-9], but wet chemistry methods can be quite expensive, particularly in the steps that involve solid-liquid separation, washing and drying [10].

Ni/NiO nanoparticles also can be synthesized in the gas phase, and several variants of this method have been used for the preparation of nickel or nickel oxide nanoparticles. In one case, Ni/NiO particles were synthesized by spray pyrolysis of water solutions of nickel precursors (e.g., nitrate, chloride, formate or acetate) but the resulting particles typically were in the submicron size range [11] or were polydisperse mixtures of nanosized particles, submicron-sized particles and, under some conditions, even supermicron-sized particles [12]. However, Lenggoro *et al.* [3] developed conditions for synthesizing NiO nanoparticles with controlled morphology by using low-pressure spray pyrolysis with a filter expansion aerosol generator [3]. Nickel nanoparticles also have been synthesized by a DC sputtering process in an argon atmosphere [13] or by a laser-assisted photonucleation process [1]. Suh *et al.* synthesized nickel nanoparticles in a tubular furnace reactor reducing $NiCl_2$ with hydrogen (present in a carrier gas) [2]. Another method for preparing Ni/NiO nanostructures is chemical vapor deposition (CVD) of metal organic precursors (MOCVD). MOCVD has a number of advantages over other methods: the process is relatively simple, it uses inexpensive equipment, and particle formation can be controlled by a variety of process parameters like reactor temperature, pre-

cursor concentration, or residence time in the reactor. An overview of Ni precursors used for CVD was presented by Brissonneau and Vahlas [14]. Promising Ni precursors for MOCVD include nickelocene [15] or nickel acetylacetonate [16].

In this work, we studied Ni/NiO nanoparticle synthesis in an externally heated tube flow reactor at moderate temperatures using nickel acetylacetonate (NiAA) as a precursor and two different methods of precursor decompositions. The goals of this study were to identify an experimental set-up suitable for the production of nickel or nickel oxide particles with valuable properties for possible applications, and to investigate the influence of process parameters on the rate of particle production and particle characteristics.

2. Experimental

Particle production was studied by two different methods of NiAA decomposition processes (**Figure 1**) [17]:

1) thermal decomposition in an inert atmosphere (pyrolysis)

$$Ni(C_5H_7O_2)_2 \rightarrow Ni + 2C_5H_7O_2, \quad (1)$$

2) reduction with hydrogen (present in the carrier gas)

$$Ni(C_5H_7O_2)_2 + H_2 \rightarrow Ni + 2HC_5H_7O_2. \quad (2)$$

Experiments were performed using the apparatus shown in **Figure 2**. Particles were synthesized in an externally heated tube flow reactor 55 cm in length and an inner diameter (i.d.) of 2.7 cm. The inlet nozzle that introduced the reaction mixture was 15 cm in length and had an i.d. of 1.5 cm. Deoxygenated (1), dry (2) and particle-free nitrogen (F) was used as the carrier gas and was saturated with NiAA vapor in an externally heated saturator (S). The precursor concentration was controlled both by the flow rate through the saturator and by the saturator temperature (T_S). The partial pressure of the precursor vapor was calculated on the basis of the experimental data of Götze *et al.* [18] from the equation

$$P_{NiAA}\,(\mathrm{Pa}) = 133.322 \times 10^{\left(10.01316 - \frac{4973.68}{T_S(\mathrm{K})}\right)} \quad (3)$$

Saturated carrier gas was fed axially through a nozzle into the center of the reactor, which was surrounded by a coaxial stream of nitrogen. In reductive decomposition experiments, the stream was composed of a mixture of nitrogen and hydrogen. The mixture of gas and particles leaving the reactor was cooled in a diluter (D) by mixing it with a stream of nitrogen gas. The saturator-reactor-diluter system was arranged vertically in this work. Flow rates of individual gas streams were controlled with electronic mass flow meters (Tesla 306 KA/RA), and the temperatures of the saturator and reactor were controlled with electronic temperature controllers (RLC T48).

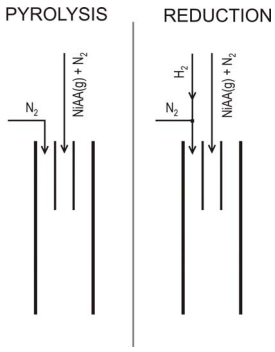

Figure 1. Scheme of the inlet arrangements for used decomposition techniques of NiAA precursor.

Particle production was monitored with a scanning mobility particle sizer (SMPS), which consisted of a TSI model 3080 electrostatic classifier (EC) and a TSI model 3025 condensation particle counter (CPC). Samples for particle characterization were deposited onto carbon-coated Cu grids by point-to-plate electrostatic precipitator or onto polytetrafluoroethylene (PTFE) or Ag filters. Samples for transmission electron microscopy (TEM) from particles deposited on filters were prepared by dispersion in an organic solvent. The resulting suspension was dropped onto a carbon-coated Cu grid. The morphology of particles was studied using two TEM instruments with different resolutions. Images from the JEOL 2010 were appropriate for characterizing overall morphology; images from the high resolution TEM (HR-

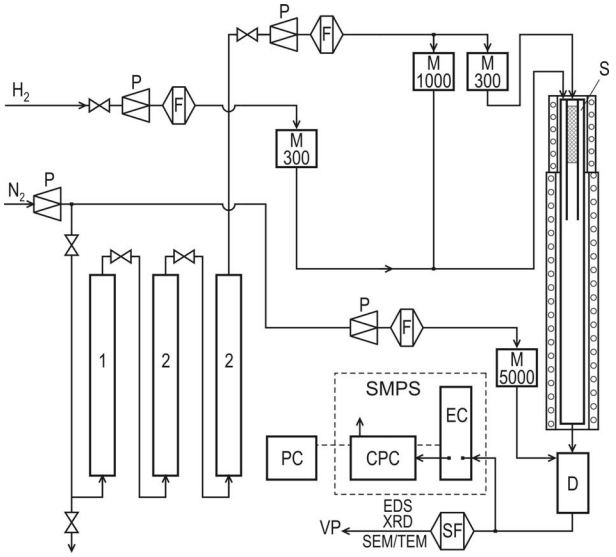

Figure 2. Scheme of the apparatus. (1) Deoxygenator, (2) Dryer, (CPC) condensation particle counter, (D) Diluter, (EC) Electrostatic classifier, (F) Filter, (M) Electronic mass flowmeter, (P) Pressure reducing valve, (S) Saturator, (SF) STERLITECH Ag filter or electrostatic precipitator, (VP) Vacuum pump.

TEM) JEOL 3010 could also distinguish details on the particle surface. The crystallinity of the particles was studied by selected area electron diffraction (SAED) and by analysis of lattice fringes detected on particles. The composition of the particles was analyzed by energy dispersive spectroscopy (EDS; Noran Vantage connected to JEOL 2010 and/or INCA/Oxford connected to JEOL 3010).

Particle production and particle characteristics were also studied by varying reactor temperature (T_R) (400˚C - 500˚C; the upper limit is set by the construction material of the reactor and furnace), reactor flow rate (Q_R, 400 - 1000 cm^3/min), hydrogen concentration (c_H, 0 vol% - 10 vol%), saturator temperature (T_S, 150˚C - 190˚C), and central nozzle flow rate (Q_{CF}, 10% - 20% of Q_R). It should be noted that Q_{CF} and T_S control the precursor concentration (P_{NiAA}). Axial temperature profile in the reactor for T_R set to 500˚C and Q_R = 0 is shown in **Figure 3**. Experimental conditions for sample preparation are summarized in **Table 1**.

3. Results

3.1. Particle Production

Particle generation was monitored by SMPS in the form of particle size distribution (PSD) curves, including the following statistics: total number concentration (N_t), geometric mean diameter (GMD), geometric standard deviation (GSD), etc. Several examples of PSD curves are shown in **Figure 4** and **Figure 5**. dN/dlogd_P represents differential number concentration, normalized to one decade of particle size. The influence of reactor temperature on particle production was studied for reductive decomposition of NiAA. Particle generation was observed at temperatures of 400˚C and higher. No particles were detected at T_R = 300˚C. For thermal decomposition, experiments were performed only at T_R = 500˚C.

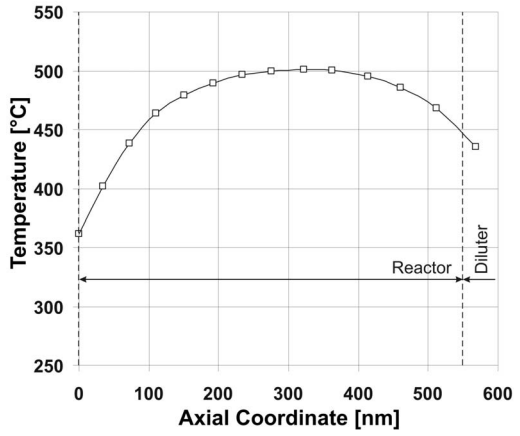

Figure 3. Axial temperature profile in the axis of the reactor for T_R set to 500˚C.

Table 1. Process parameters of the samples for particle characterization.

Sample No.	T_R [˚C]	T_S [˚C]	Q_R [cm^3/min]	P_{NiAA} [Pa]	c_H [vol%]	Rem.
NiAA4	500	180	900	2.9	0	PYROLYSIS
NiAA7	400	180	800	2.9	10	REDUCTION
NiAA8	500	180	800	2.9	7	REDUCTION
NiAA9	500	180	600	2.9	7	REDUCTION
NiAA10	500	180	800	2.9	10	REDUCTION
NiAAF1	500	150	800	0.48	0	PYROLYSIS
NiAAF2	500	180	800	2.9	0	PYROLYSIS

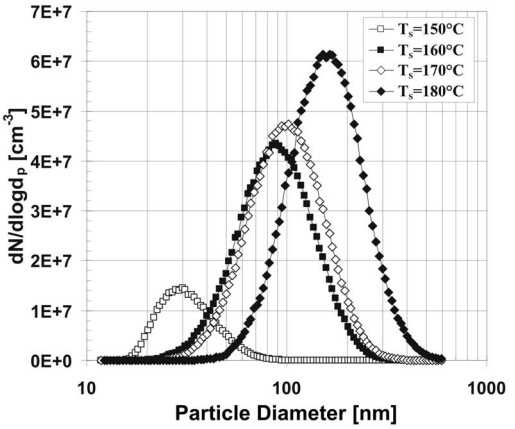

Figure 4. Influence of T_S on PSD at T_R = 500˚C, Q_R = 800 cm^3/min, Q_{CF} = 20% Q_R, pyrolysis.

Generally, particle production (mean particle size and number concentration) increases with increasing saturator temperature (T_S) (**Figure 4**). The particle concentration increased from 4.92 × 10^6 cm^{-3} at T_S = 150˚C to 2.85 × 10^7 cm^{-3} at 180˚C. Values of GMD at these T_S values were 32 and 156 nm, respectively, and the GSD values were 1.37 and 1.52, respectively. **Figure 5** shows the

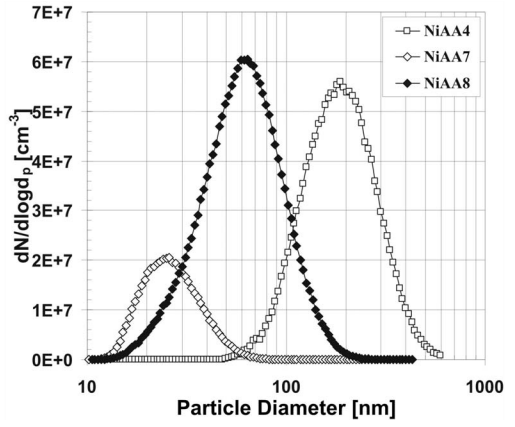

Figure 5. Particle size distributions corresponding to TEM samples NiAA4, NiAA7 and NiAA8. Experimental conditions are shown in Table 1.

influences of the precursor decomposition method and the reactor temperature; the remaining conditions in these experiments were nearly identical (**Table 1**). It is evident that the rate of particle formation by reduction of NiAA at 400˚C (NiAA7) is much lower (N_t = 7.48 × 10^6 cm^{-3}, GMD = 26 nm, GSD = 1.38) than that at 500˚C (NiAA8, N_t = 2.96 × 10^7 cm^{-3}, GMD = 59 nm, GSD = 1.58). At 500˚C, the mean particle size for reductive precursor decomposition (NiAA8) was smaller than those for thermal decomposition (NiAA4, N_t = 2.58 × 10^7 cm^{-3}, GMD = 185 nm, GSD = 1.51) (**Figure 5**). The other parameters in **Table 1**, *i.e.* reactor flow rate and/or hydrogen concentration variation from 7 to 10 vol%, had not remarkable effect on particle production.

3.2. Particle Characteristics

3.2.1. Pyrolysis

The morphology of particles prepared by pyrolysis of NiAA can be seen in **Figure 6**. The particles have shell-like structures, the mean size of the primary particles is well below 50 nm and they are arranged into clusters and/or chains. The samples (NiAAF1, NiAAF2) deposited on PTFE filter are dark in color, suggesting that they may be contaminated by carbon from incomplete decomposition of the precursor. Formation of carbon-coated Ni nanoparticles by thermal decomposition of solid nickel acetate in a closed Swagelok reactor was observed by Pol *et al.* [19]. Electron diffraction pattern (EDP) in **Figure 6** is due to small particle size rather weak. Nevertheless, there are two recognizable rings in the EDP that correspond to interplanar spacings of 0.205 nm and 0.189 nm, respectively. There are also less-visible dots that correspond to spacings of 0.176 nm, 0.123 nm and 0.106 nm. These values may represent d_{111} = 0.203 nm, d_{200} = 0.176 nm, d_{220} = 0.125 nm, d_{311} = 0.106 nm of face centred cubic (FCC) Ni (PDF ICDD 4-0850). The spacing 0.205 nm is also consistent with d_{200} = 0.208 nm FCC NiO (4-0835) and 0.123 nm is consistent with d_{311} = 0.126 or d_{222} = 0.121 nm of FCC NiO, but there are missing rings or dots corresponding to d_{111} and d_{220} NiO. The spacing 0.189 nm does not fit with any interplanar spacing of either FCC Ni or FCC NiO. HRTEM images enabled a more detailed analysis of particle morphology, crystallinity and, therefore, particle composition. **Figure 7** shows HRTEM images of particles of sample NiAAF1. We can see lattice fringes d_{111} of FCC Ni (4-0850), see area A and corresponding fast Fourier transformation (FFT) pattern in **Figure 7(a)** and d_{105} of hexagonal NiOOH (6-0075) (see area B and corresponding FFT in **Figure 7(a)**. The crystalline structure of hexagonal NiOOH (6-0075) and FCC NiO (22-1189) can be seen in **Figure 7(b)**. As inset, there is FFT pattern of cubic NiO crystalline structure along [–300]c zone axis. EDS analysis (INCA Oxford) was applied to the samples NiAAF1 and NiAAF2, deposited on filters. The diameter of the spot area varied from ~5 nm to ~30 nm, and O/Ni (atomic%) ratios of 0.38 to 1.86 were obtained. Because the sensitivity of EDS to individual elements of the periodic table depends on the atomic number, the values of the O/Ni ratio do not reflect stoichiometry. Furthermore, the O/Ni ratio could be affected (increased) during the preparation of TEM samples from the particles deposited on filters.

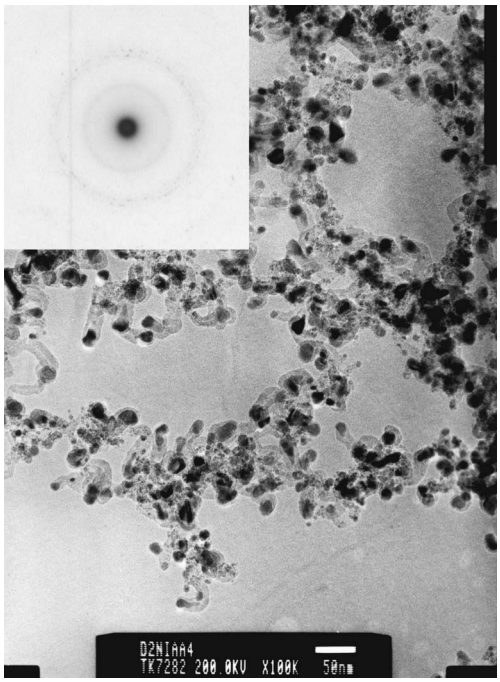

Figure 6. Bright field TEM image and SAED pattern of particles prepared by pyrolysis of NiAA, sample NiAA4: T_R = 500˚C, T_S = 180˚C, Q_R = 900 cm^3/min.

3.2.2. Reduction of NiAA

The morphology of particles obtained by reduction differs significantly from those produced by thermal decomposition and depends also on the reactor temperature. At T_R = 400˚C, primary particles 10 - 15 nm in size were agglomerated into clusters and/or chains, and they had

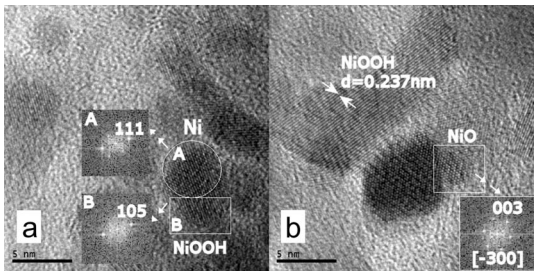

Figure 7. HRTEM images and FFT patterns of particles prepared by pyrolysis of NiAA, sample NiAAF1: T_R = 500˚C, T_S = 150˚C, Q_R = 800 cm^3/min.

also faintly shell-like structures (**Figure 8**). Particles produced at 500˚C had slightly broader size distribution (from 10 nm to ca. 50 nm) and samples consisted of separated nanoparticles of various sizes from the aforementioned range as well as from clusters of small nanoparticles (~10 nm) **(Figure 9**). The shell-like structure almost disappeared. Particles produced at 400˚C were amorphous, while those synthesized at 500˚C were crystalline. Two EDPs taken by the JEOL 2010 are shown in **Figure 9**. The EDP of the cluster of nanoparticles is visible on the left-hand side of **Figure 9**. The innermost ring corresponds to d_{111} of FCC NiO (0.241 nm), the third to d_{220} FCC NiO (0.145 nm), while the middle resolvable ring (0.206 nm) can be attributed both to d_{111} FCC Ni and to d_{200} FCC NiO, so it is probable that both crystalline structures are present in the sample. The EDP of a single crystal of FCC Ni from approximately 50 nm nanoparticle is apparent on the right-hand side of **Figure 9**.

Results obtained by SAED are in qualitative agreement with those obtained by EDS. EDS analyses showed an oxygen to nickel ratio (atom%) of 3.0 in the cluster of nanoparticles from **Figure 9(a)**, while the ratio was only 0.23 in the large particle of **Figure 9(b)**. The value of O/Ni ratio in the sample NiAA7 (400˚C) was 0.89.

Several samples of particles prepared by reduction were also analyzed using HRTEM, which enabled detection of the lattice fringes of several of Ni/NiO_x crystalline structures. **Figures 10(a-c)** show the lattice fringes of cubic NiO (4-0835) with an interplanar spacing of d_{200} = 0.208 nm, as well as lattice fringes of cubic Ni (4-0850) with an interplanar distance of d_{111} = 0.203 nm and the hexagonal lattice structure of NiOOH (6-0075), confirmed by FFT pattern along the [006]c zone axis. A detailed analysis of the crystalline particle of the sample NiAA10 (**Figure 10(d)**) shows FCC Ni (4-0850) in the bulk and a NiO/NiOOH crystalline structures on the surface. As inset, there is a FFT pattern of a typical cubic Ni along the [02-2] axis.

Comparing lattice fringe images and SAED patterns, we can conclude that the particles consist of a metallic Ni core and a thin surface layer composed of NiO/NiOOH crystalline structures. These observations are in agreement with those of Uchikoshi *et al.* [20]. Ni core and NiO shell nanoparticles produced by DC sputtering were reported by Rellinghaus *et al.* [13].

4. Discussion

From a comparison of TEM images with PSD curves, it is evident that SMPS detected already agglomerated primary particles. The size of primary particles on TEM images is much smaller than indicated by the PSD curves in **Figure 5**. In spite of this, SMPS still provides useful information about the particle formation process. The curves in **Figure 5** are in good qualitative agreement with the particle morphology shown in the TEM images. Particles synthesized by reduction at 400˚C (**Figure 8**) are the smallest, and their clusters are much smaller than those of the other samples (PSD curve NiAA7 in **Figure**

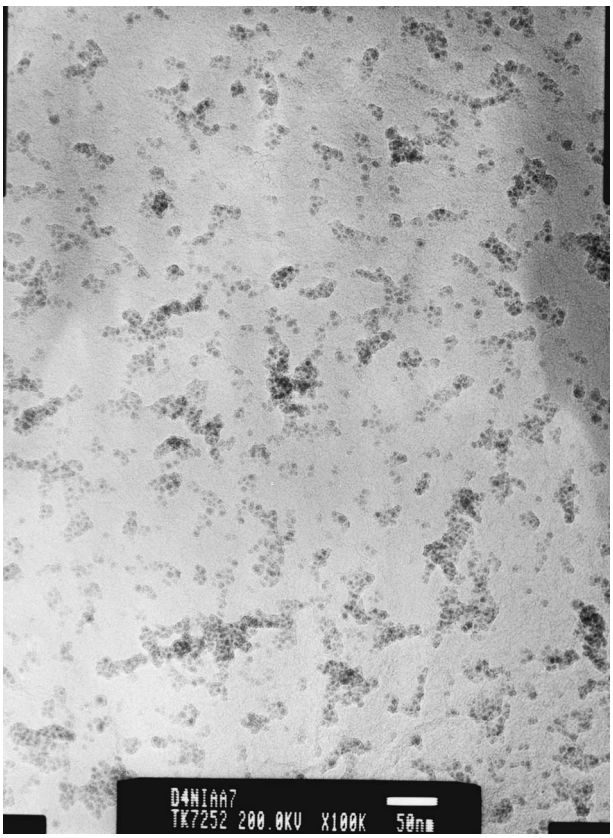

Figure 8. Brigth field TEM image of particles produced by reduction of NiAA, sample NiAA7: T_R = 400˚C, T_S = 180˚C, Q_R = 800 cm^3/min, c_H = 10 vol%.

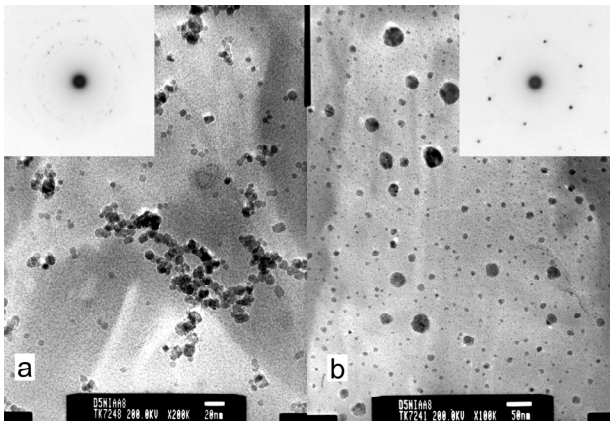

Figure 9. Bright field TEM images and SAED patterns of particles produced by reduction of NiAA, sample NiAA8: T_R = 500˚C, T_S = 180˚C, Q_R = 800 cm^3/min, c_H = 7 vol%.

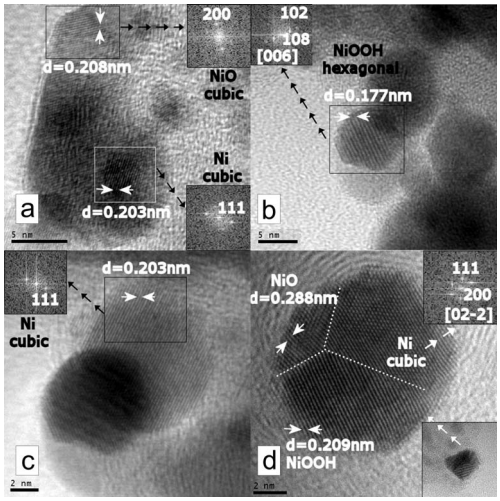

Figure 10. HRTEM images and FFT patterns of particles prepared by reduction of NiAA, a-c; sample NiAA9: T_R = 500˚C, T_S = 180˚C, Q_R = 600 cm^3/min, c_H = 7 vol%, d; sample NiAA10: T_R = 500˚C, T_S = 180˚C, Q_R = 800 cm^3/min, c_H = 10 vol%.

5). And particles prepared by reduction of NiAA at 500˚C (**Figure 9**) have slightly broader size distribution than those prepared by pyrolysis (**Figure 6**), but they are less aggregated, which corresponds to the much smaller mean particle size indicated by PSD curve NiAA8 in **Figure 5**.

The shell-like structure of particles seen in samples NiAA4 (**Figure 6**), and somewhat in NiAA7 (**Figure 8**) seems to be formed from incomplete decomposition of the precursor by pyrolysis T_R = 500˚C, and also by reduction at T_R = 400˚C, respectively. This incomplete decomposition is suggested by the fact that deposits of particles from pyrolysis on the PTFE filter were dark in color, while those from reduction at 500˚C were silver in color. Furthermore, it seems that the shell layer also protects particles against oxidation. The O/Ni ratio was lower in the samples of particles with shell-like structures: 0.38 - 1.86 in sample NiAA4 (pyrolysis) and 0.89 in sample NiAA7 (reduction, 400˚C), while in the particles without a shell (NiAA8; reduction, 500˚C), it was 3.0. However, the O/Ni ratio also depends on particle size. The lowest value of the O/Ni ratio (0.23) was detected in spot analysis of the large particle in sample NiAA8, and this low value can be attributed to the small surface-to-volume ratio of the relatively large particle.

5. Conclusions

Ni/NiO_x nanoparticles were synthesized by pyrolysis and reduction of NiAA in an externally heated tube flow reactor. Particle production was observed at T_R = 400˚C and above, and depends mainly on T_R, P_{NiAA} and the type of precursor decomposition method. The size range of primary particles varied from ~10 nm to ~50 nm, and they typically were somewhat agglomerated. Particles prepared by pyrolysis had shell-like structure, and were aggregated into clusters and/or branched chains. EDP consists predominantly of rings or dots characteristic of FCC Ni, while HRTEM lattice images showed lattice fringes of both FCC Ni and NiO, and also of NiOOH. Results obtained by SAED are in qualitative agreement with those obtained by EDS (O to Ni ratio).

Particles produced by reduction differ significantly in morphology, crystallinity and composition. These particles had slightly broader size distribution, they were less agglomerated and the shell-like structure was almost nonexistent. EDPs vary with particle size. SAED, EDS and HRTEM lattice fringes images suggest that particles consist of a metallic core with a surface layer composed of various oxide forms of Ni (NiO, NiOOH).

6. Acknowledgements

This work was supported by the Grant Agency of the Czech Republic No. 104/07/1093 and by the Finnish Academy of Sciences and Letters. Some TEM/EDS analyses were performed by Tomi Kanerva, Institute of Material Science, Tampere University of Technology.

REFERENCES

[1] H. He, R. H. Heist, B. L. McIntyre and T. N. Blanton, "Ultrafine Nickel Particles Generated by Laser-Induced Gas Phase Photonucleation," *NanoStructured Materials*, Vol. 8, No. 7, 1997, pp. 879-888. doi:10.1016/S0965-9773(98)00016-6

[2] Z. J. Suh, H. D. Jang, H. K. Chang, D. W. Hwang and H. C. Kim, "Kinetics of Gas Phase Reduction of Nickel Chloride in Preparation for Nickel Nanoparticles," *Materials Research Bulletin*, Vol. 40, No. 12, 2005, pp. 2100-2109. doi:10.1016/j.materresbull.2005.07.004

[3] I. W. Lenggoro, Z. Itoh, N. Iida and K. Okuyama, "Control of Size and Morphology in NiO Particles Prepared by a Low-Pressure Spray Pyrolysis," *Materials Research Bulletin*, Vol. 38, No. 14, 2003, pp. 1819-1827. doi:10.1016/j.materresbull.2003.08.005

[4] D. Tao and F. Wei, "New Procedure towards Size-Homogeneous and Well-Dispersed Nickel Oxide Nanoparticles of 30 nm," *Materials Letters*, Vol. 58, No. 25, 2004, pp. 3226-3228. doi:10.1016/j.matlet.2004.06.015

[5] C. G. Granqvist, "Handbook of Inorganic Electrochromic Materials," Elsevier, Amsterdam, 2002, pp. 339-375.

[6] S. V. Kumari, M. Natarajan, V. K. Vaidyan and P. Koshy, "Surface Oxidation of Nickel Thin Films," *Journal of Materials Science Letters*, Vol. 11, No. 11, 1992, pp. 761-762. doi:10.1007/BF00729484

[7] X. Li, X. Zhang, Z. Li and Y. Qian, "Synthesis and Characterization of NiO Nanoparticles by Thermal Decomposition of Nickel Dimethylglyoximate Rods," *Solid State Communications*, Vol. 137, No. 11, 2006, pp. 581-

584. doi:10.1016/j.ssc.2006.01.031

[8] G. G. Couto, J. J. Klein, W. H. Schreiner, D. H. Mosca, A. J. A. de Oliveira and A. J. G. Zarbin, "Nickel Nanoparticles Obtained by a Modified Polyol Process: Synthesis, Characterization, and Magnetic Properties," *Journal of Colloid and Interface Science*, Vol. 311, No. 2, 2007, pp. 461-468. doi:10.1016/j.jcis.2007.03.045

[9] T. A. Dobbins, D. Poondi and J. Singh, "Synthesis of Micron and Submicron Nickel and Nickel Oxide Particles by a Novel Laser-Liquid Interaction Process," *Journal of Materials Synthesis and Processing*, Vol. 7, No. 5, 1999, pp. 261-271. doi:10.1023/A:1021864719176

[10] K. Wegner and S. E. Pratsinis, "Gas-Phase Synthesis of Nanoparticles: Scale-up and Design of Flame Reactors," *Powder Technology*, Vol. 150, No. 2, 2005, pp. 117-122. doi:10.1016/j.powtec.2004.11.022

[11] D.-J. Kang, S.-G. Kim and H.-S. Kim, "Morphologies and Properties of Nickel Particles Prepared by Spray Pyrolysis," *Journal of Materials Science*, Vol. 39, No. 18, 2004, pp. 5719-5726. doi:10.1023/B:JMSC.0000040081.43634.31

[12] K.-Y. Jung, J.-H. Lee, H.-Y. Koo, Y.-C. Kang and S.-B. Park, "Preparation of Solid Nickel Nanoparticles by Large-Scale Spray Pyrolysis of $Ni(NO_3)_2 \cdot 6H_2O$ Precursor: Effect of Temperature and Nickel Acetate on the Particle Morphology," *Materials Science and Engineering B*, Vol. 137, No. 1-3, 2007, pp. 10-19. doi:10.1016/j.mseb.2006.09.025

[13] B. Rellinghaus, S. Stappert, E. F. Wassermann, H. Sauer and B. Spliethoff, "The Effect of Oxidation on the Structure of Nickel Nanoparticles," *The European Physical Journal D*, Vol. 16, No. 1, 2001, pp. 249-252. doi:10.1007/s100530170103

[14] L. Brissonneau and C. Vahlas, "Precursors and Operating Conditions for the Metal-Organic Chemical Vapor Deposition of Nickel Films," *Annales de Chimie-Science des Materiaux*, Vol. 25, No. 2, 2000, pp. 81-90. doi:10.1016/S0151-9107(00)88716-4

[15] L. Brissonneau and C. Vahlas, "MOCVD-Processed Ni Films from Nickelocene. Part I: Growth Rate and Morphology," *Chemical Vapor Deposition*, Vo. 5, No. 4, 1999, pp. 135-142. doi:10.1002/(SICI)1521-3862(199908)5:4<135::AID-CVDE135>3.0.CO;2-1

[16] T. Maruyama and T. Tago, "Nickel Thin Films Prepared by Chemical Vapour Deposition from Nickel Acetylacetonate," *Journal of Materials Science*, Vol. 28, No. 9, 1993, pp. 5345-5348. doi:10.1007/BF00570088

[17] T. T. Kodas and M. J. Hampden-Smith, "Aerosol Processing of Materials," Wiley-VCH, New York, 1999, p. 203.

[18] H.-J. Götze, K. Bloss and H. Molketin, "Dampfdruckbestimmung von Acetylacetonaten," *Zeitschrift für Physikalische Chemie Neue Folge*, Vol. 73, No. 4-6, 1970, pp. 314-320. doi:10.1002/ejic.200700146

[19] S. V. Pol, V. G. Pol, I. Felner and A. Gedanken, "The Thermal Decomposition of Three Magnetic Acetates at Their Autogenic Pressure Yields Different Products. Why?," *European Journal of Inorganic Chemistry*, Vol. 2007, No. 14, 2007, pp. 2089-2096. doi:10.1002/ejic.200700146

[20] T. Uchikoshi, Y. Sakka, M. Yoshitake and K. Yoshihara, "A Study of the Passivating Oxide Layer on Fine Nickel Particles," *NanoStructured Materials*, Vol. 4, No. 2, 1994, pp. 199-206. doi:10.1016/0965-9773(94)90078-7

